COMPLEX-SURFACED OBJECTS: EFFECTS ON PHASE AND AMPLITUDE IMAGES IN PULSED PHASE THERMOGRAPHY

C. Liu[1], L. Czuban[1], P. Bison[2], E. Grinzato[2], S. Marinetti[2], X. Maldague[1]

[1]Electrical and Computing Engineering Department [maldagx@gel.ulaval.ca]
Université Laval, Québec City (Québec) G1K 7P4, Canada
[2]CNR-ITC, Corso Stati Uniti 4, 35127 Padova (Italy)

Abstract

Pulsed phase thermography (PPT) is a common approach in non-destructive testing by infrared thermography. In PPT, data analysis applies the Discrete Fourier transform (DFT) to thermal images obtained in pulsed infrared thermography (PT) to compute phase and amplitude images in the frequency domain. In this paper, influence of complex surfaces on images in the frequency domain is studied. It is known that complex-surfaced objects have their corresponding PT images affected due to non-uniform heating and emission. For phase images, inversion analysis proceeds with the known *blind frequency* approach and it is shown such an analysis is still suitable in case of complex-shaped objects. In case of amplitude images, a relationship between complex-shaped surfaces and corresponding amplitude data is proposed. Detailed analysis methods and experimental results are presented.

1. Introduction

Pulsed phase thermography (PPT) is a common processing method in pulsed infrared thermography (PT) [1]. In PPT, data analysis relies on the Discrete Fourier transform (DFT). Following the DFT, two kinds of images are available in the frequency domain: phase and amplitude images. Phase images are used to analyze subsurface defect features since phase is sensitive to inconsistent material properties under specimen surface. Moreover, it is known phase images are little affected by surface features, such as the non-uniform heating deposited on the specimen surface. On the other hand, amplitude images are affected by surface features while they probe a limited depth under specimen surface. Thus, phase and amplitude images have different applications and limitations in PT.

In this paper, complex-shaped specimens are studied in PT. In PT, the IR camera and the heating source are located in front of the specimen (reflection scheme), thus obviously parallel parts of the specimen receive and emit more energy than perpendicular parts. All to say in PT complex-shaped objects exhibit a thermal behavior which depends on their shape. In this paper, we focus on these influences in the case of phase and amplitude images obtained in PT after PPT processing.

For phase images, we want to verify if the analysis based on the *blind frequency* concept still hold for complex-shaped surfaces [1]. For amplitude images, the analysis focuses on the possible relationship between specimen surface shape and amplitude images. We developed a method called “shape from amplitude” adapted from the method of “shape from heating” reported by Barker *et al.*, [2] and Pelletier *et al.*, [3].

2. Background theory

2.1. Pulsed phase thermography (PPT)

PPT was by developed by Maldague and Marinetti [4]. It combines advantages of PT and modulated thermography (MT). The experimental procedure is as follows. The heating source launches a short pulse of heat on the surface of the specimen (PT approach). Computation of PPT relies on the one-dimensional DFT whose expression is:

$$F_n = \sum_{k=0}^{N-1} T(k) e^{2pikn/N} = \mathrm{Re}_n + i\,\mathrm{Im}_n \qquad (1)$$

where i is the imaginary number, Re_n and Im_n present respectively the real and imaginary components of F_n, and n is the discrete frequency increment. The expressions of phase and amplitude are thus:

$$f_n = \tan^{-1}\left(\frac{\mathrm{Im}_n}{\mathrm{Re}_n}\right) \qquad (2)$$

$$A_n = \sqrt{\mathrm{Im}_n{}^2 + \mathrm{Re}_n{}^2} \quad (3)$$

2.2. Thermal wave theory

Thermal waves are highly attenuated and dispersive waves which are generated inside the material. Those were first investigated by J. Fourier and A. J. Ångström [5, 6]. The thermal wave phenomenon is the response of the specimen to a periodic heat source.

For a planar specimen, a temperature field with a thermal wave could be expressed as follows:

$$T(x,t) = A\cos(\nu t - f) = T_o e^{-\frac{z}{m}} \cos(\nu t - \frac{2pz}{l}) \quad (4)$$

where x is the depth of the temperature field (x=0 corresponds to the periodical heat generated at the surface), t is the transport time, A is the amplitude of the thermal wave, f is its phase, T_o is the initial surface temperature, and z is the depth reached by the thermal wave.

According to Eq.(4), phase of the thermal wave is expressed as:

$$f(z) = \frac{z}{m} \quad (5)$$

where μ is the thermal diffusion length. From the above equation, it is noticed phase is mostly related to z and μ without being much affected by other parameters.

3. Influence of complex surfaces on phase images

Analysis of phase images is based on the *blind frequency* concept which is a known inversion technique for defect quantification [1]. The blind frequency is the frequency for which a defect at a given depth becomes firstly visible in the frequency spectrum. From Eq.(2) and Eq.(5), it is shown that phase images are sensitive to inconsistent material properties inside the specimen while they are little affected by thermal noise on objects surfaces thanks to the ratio of the expression in Eq. (2). The expression linking the blind frequency to the depth is as follows [1]:

$$z \approx 1.8\sqrt{\frac{a}{pf_b}} \quad (6)$$

where z is the depth of the considered subsurface defect, 1.8 is a constant, α is the thermal diffusivity and f_b is the blind frequency [4].

From Eq.(6), it is seen the blind frequency relies mostly on α and z and thus it should not be much affected by the surface shape.

4. Shape from amplitude

For amplitude images, our goal is to establish a relationship between surface orientation of a complex-shaped object and its amplitude image at a given frequency. It is known that complex surface affects thermal images since different surface orientations receive and emit different thermal energies. As stated above, surfaces parallel to the IR camera and heating source plane receive and emit more energy than areas perpendicular to it which receive only little energy. Since directly related to the thermal images following Eq. (3), amplitude images are thus directly related to surface shape of inspected objects.

The proposed calculation method of how to extract a 3D surface shape from an amplitude image is based on the method of "shape from heating" reported by Barker *et al.*, [2] and Pelletier *et al.*, [3]. More details are found into those references. "Shape from heating" method extracts surface shape from the first thermal image recorded in time. It mainly includes three steps: 1- image segmentation, 2- region growing and 3- shape extraction. In our case, we apply this method on amplitude images and the analyzed image is chosen at a low frequency (even the lowest), since most of the energy is concentrated at low frequencies [4].

4.1. Image segmentation

Before applying the method of "shape from heating" on an amplitude image, we need to extract the background information, this step is called "background extraction". On amplitude images, deeper subsurface defects always appear at lower frequencies and this obviously affect shape extraction [4]. The goal of background extraction is then to remove the effect of these defects, but keep the whole trend of the background. A robust smooth fitting approach [7] is thus performed line by line on the analyzed image for such a purpose.

Next, we apply edge detection on the analyzed

image to avoid edge effects in further analysis. A Sobel or Canny filter is used for this purpose. After that procedure, a quadric square fitting is carried out to smooth the image [3]. The expression of this fitting is as follows:

$$Am(x, y) = Ax + By + C \quad (7)$$

where *Am* is the amplitude value of each pixel, *A*, *B* are the gradients along the *x*, *y* directions, and *C* is the average amplitude value of the corresponding window. These parameters *A*, *B* and *C* represent values for each pixel on the image.

The next step is to divide the smoothed image into small patches. The size of a patch depends on the quality of the image, usually a size of 5 by 5 pixels is appropriate.

Once the image has been divided into patches, we classify these patches into *linear* or *nonlinear* classes. It is known that on a complex surface, variations for a linear part is much different from that of a nonlinear part. A linear part is more concerned by variations of relative depth while for a nonlinear part, surface orientation is the main variation. For this reason, a classification criterion is used to classify patches. The criterion relies on two calibration parameters: *S* and *d*. *S* is the ratio of the variation of amplitude value to the relative depth, and *d* is the distance covered by one pixel. The product $S \cdot d$ represents the variation of amplitude in the image. Expression of this criterion is as follows:

$$(A \text{ and } B) \le S \cdot d \quad (8)$$

If (*A* and *B)* is lower than or equal to this threshold, the patch is classified as belonging to a *linear* class, otherwise it is classified as *a non-linear* class.

4.2. Region growing

The purpose of region growing is to merge neighbor patches which have similar properties in order to make greater uniform regions (thus reducing also the noise).

Firstly, we need to choose a seed patch to begin the region growing. The patch having the maximum *E* is chosen as the seed:

$$E = \frac{n}{e \cdot n + 1} \quad (9)$$

where *n* is the number of available neighbor patches around the studying pixel, ε is the error between non-processed and smoothed patches. Once the maximum *E* has been chosen as seed patch, region growing begins at this location.

A 8-neighbor connectivity study is carried out by comparing the coefficients (*A*, *B* and *C*) of the studied patch with those of the seed. If the difference is lower than a given threshold, then the patch is merged into the current region and all coefficients in the region are averaged together. The processing continues until no pixel could be merged into the region. Then a new process starts again with another selected seed. It stops when all the pixels in the image are accepted within a region

4.3. Shape extraction

The last step is to extract shape information. It is divided into "extraction of relative depth" and "extraction of surface orientation". The former is applied to linear classes, while the later is performed on nonlinear classes.

For linear classes, before to extract relative depth, we should remove effects of surface orientation. According to gradients *A*, *B* and calibration parameters *S* and *d*, the corresponding surface orientation can be computed as:

$$q_{x,y} = \sin^{-1}\left(\frac{A \text{ or } B}{S \cdot d}\right) \quad (10)$$

where $q_{x,y}$ is the orientation calculated from the calibration. However, in order to calculate the real surface orientation, two partial derivatives *p* and *q* are also needed. The real surface orientation φ is the surface orientation between the normal direction and the heating direction. Thus, expressions of real surface orientation φ can be expressed as follow:

$$\begin{cases} p = \dfrac{\Delta z}{\Delta x} = \tan q_x \\ q = \dfrac{\Delta z}{\Delta y} = \tan q_y \end{cases} \quad (11)$$

$$j = \tan^{-1}(p^2 + q^2)^{1/2} \quad (12)$$

where *p* is the partial derivative in x-direction, *q* is the partial derivative in y-direction.

Once surface orientation φ is obtained, in order to extract surface depth information, we should remove effects of φ from the image. The required

expression is as follows [2]:

$$Am_{eq} = \frac{Am}{\cos j} \quad (13)$$

where Am_{eq} is the amplitude value "cleaned" from the influence of the surface's orientation. The relative surface depth z is then expressed as:

$$z = \frac{Am_{eq} - Am_{eq(ref)}}{S} \quad (14)$$

where $Am_{eq(ref)}$ is the pixel having the highest amplitude value. This pixel is chosen as the reference pixel. Other pixels in the image compare to it. Am_{eq} is the pixel of interest.

For nonlinear classes, relative depth *z* is not an important element, because the main surface changes come from the local surface orientation. Here, variations of depth can be ignored. Hence, we are only concerned by variations of surface orientation in a non-linear surface case. The calculation φ is as follows:

$$j = \cos^{-1}\left(\frac{Am}{Am_{\max}}\right) \quad (15)$$

where *Am* is the amplitude at the pixel of interest, Am_{max} is the maximum amplitude value in the image, which is chosen as the reference pixel. Other pixels compare to it.

5. Results of image analysis

5.1. Results with phase images

In order to test if the blind frequency is affected by complex surface shape, we performed a series of experiments by tilting a Plexiglass™ plate specimen to different orientations in front of the PT set-up as shown on Fig.1.

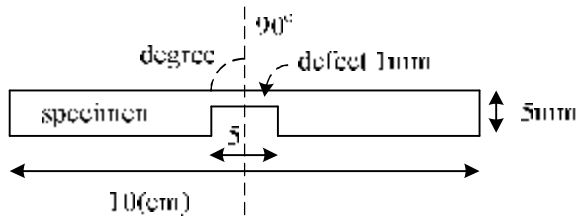

Fig.1: *Plexiglas specimen tilted to different orientations.*

First of all, we analyzed the blind frequencies from the phase curves. Fig. 2 shows phase curves of the specimen tilted to: 0°, 30° and 65°. The corresponding blind frequencies are respectively: 0.132, 0.115 and 0.125 Hz. Table 1 presents the blind frequency with different rotations of the specimen. It seems that the blind frequency is little affected by variations of the surface.

Table 1: *Blind frequency values when specimen is rotated to different orientations.*

Degree (°)	Blind frequency
0	0.132
10	0.117
20	0.118
30	0.115
40	0.110
50	0.120
60	0.121
65	0.125
70	0.088[1]

When the specimen is tilted above 50°, blind frequency is not well extracted due to the high noise level. As shown on Fig.2 (a), (b) and (c), the noise increases while increasing the specimen rotation. "Thermography signal reconstruction" (TSR) is applied to solve this problem [8]. In TSR, authors propose to fit the temperature decay curve with a polynomial since it follows a straight-line decay on a logarithmic scale (with a corresponding -½ slope). The main idea of the TSR is to generalize a straight line (i.e. a first degree polynomial) to a k^{th} degree polynomial. Generally, a 4^{th} degree or a 5^{th} degree is good enough to fit the data [8]. In our experiments, we used a 5^{th} degree polynomial. The corresponding expression is as follows:

$$\ln(\Delta T) \approx a_0 + a_1 \ln(t) + a_2 \ln^2(t) + a_3 \ln^3(t) + a_4 \ln^4(t) + a_5 \ln^5(t) \quad (16)$$

Once the temperature curve has been fitted with such a procedure, we use the so-called "synthetic temperature data" (i.e. the fitted data) to perform the Fourier transform. Therefore, we obtain a "new" phase curve which is quite exempt from noise but nevertheless keeps the curve trend. This step avoids loss information on phase curves.

[1] is abnormal data. It is possibly disturbed by high level noises.

Table 2: *Blind frequency with different orientations for fitted phase curves.*

Degree	Blind frequency
0	0.134
10	0.121
20	0.122
30	0.120
40	0.115
50	0.132
60	0.122
65	0.120
70	0.115

Table 2 presents results of blind frequency for fitted phase curves. Fig.3 shows phase curves for the specimen tilted to: 0°, 30° and 65°. The corresponding blind frequencies are 0.134, 0.120 and 0.120 Hz.

From all those phase curves, we notice blind frequencies do not change with orientation of surface. Hence, we might say that the *blind frequency inversion approach still holds even when the inspected object has a complex-surface.*

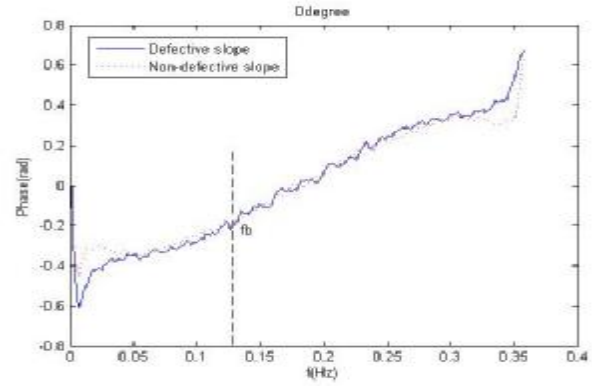

(a)

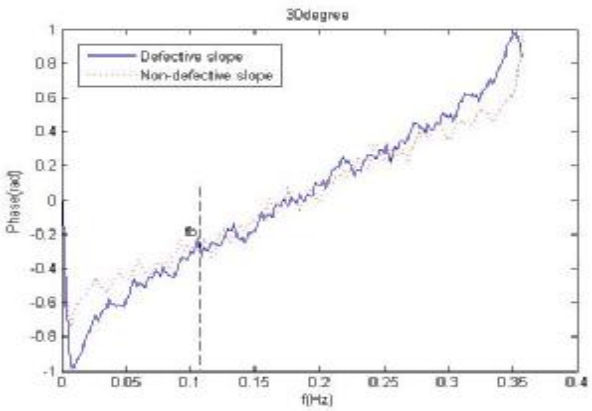

(b)

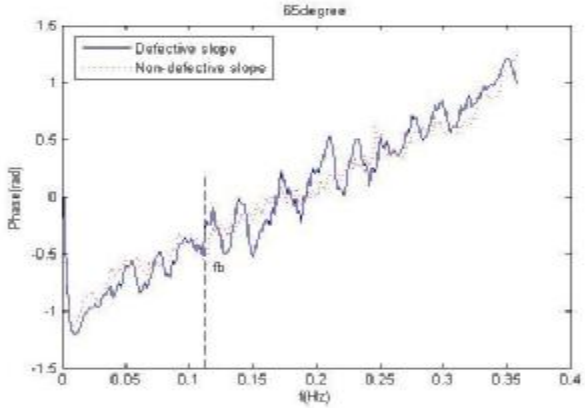

(c)

Fig.2: *Phase curves*[2] *with blind frequencies: (a) 0°; (b) 30°; (c) 65°.*

5.2. Results with amplitude images

To perform "shape from amplitude", a trapezoidal GFRP (Glass Fiber Reinforced Plastic) specimen was taken as a linear example. Height of this trapezoid is 6 cm. The two angles of the trapezoid are 30.9°. Fig.4 shows the real surface shape and extracted results. Fig.4 (a) shows the image of the real model of this object, Fig.4 (b) is the extracted surface shape, Fig.4 (c) presents the average profiles of these two shapes. The average error between real and ideal

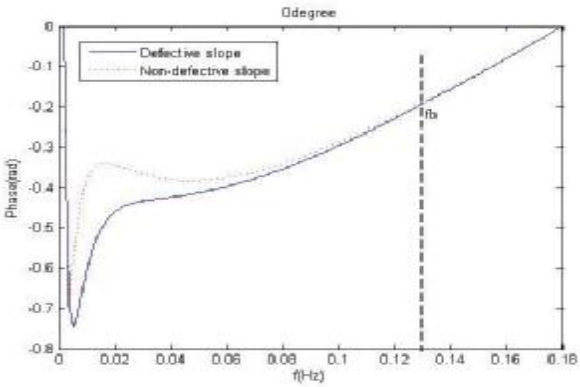

(a)

[2] a simple smooth function was performed on phase curves to remove the noise.

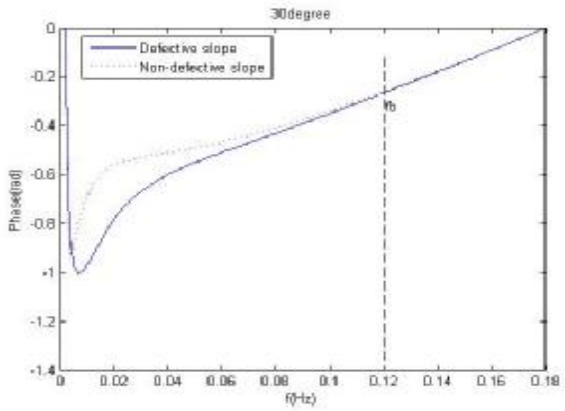

(b)

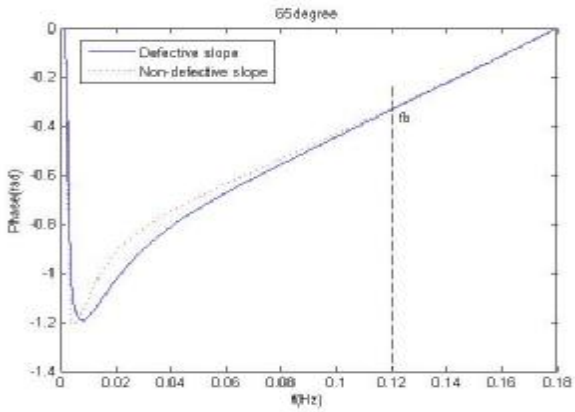

(c)

Fig.3: *Fitted phase curves with blind frequencies: (a) 0 degree; (b) 30 degrees; (c) 65 degrees.*

surface is about 0.117 cm. The analyzed imagewas the amplitude image at the first discrete frequency (f = 0.0443 Hz).

An hemicycle plexiglas specimen (radius = 4.6 cm) is used to study the non-linear case. Fig.5 shows the results: Fig.5 (a) is the image of the real surface orientations, Fig.5(b) presents the image of the extracted object surface, Fig.5(c) shows the average profile of the error between real and extracted surface. The mean error of orientation is about 4.0^{o}. The analyzed image was the amplitude image at f = 0.0418 Hz.

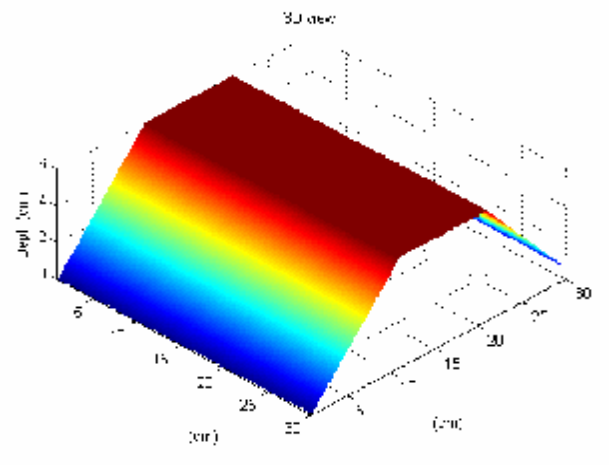

(a)

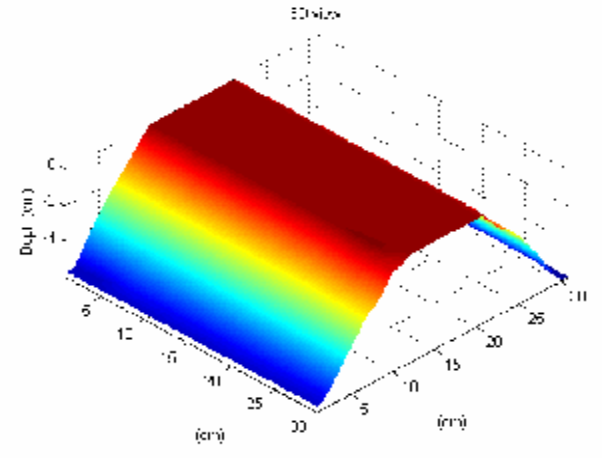

(b)

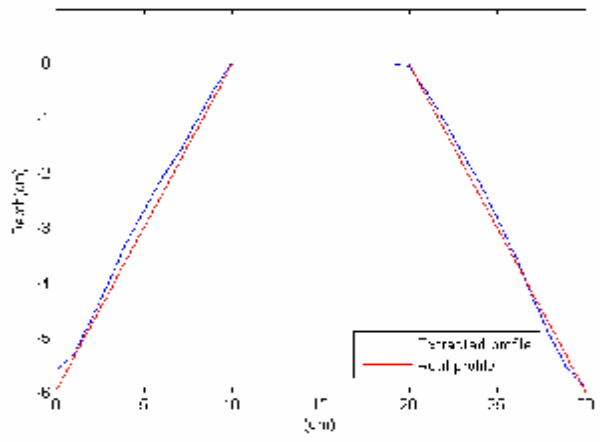

(c)

Fig.4: *A GFRP trapezoidal specimen: (a) real surface shape; (b) extracted surface shape; (c) mean profiles of (a) and (b).*

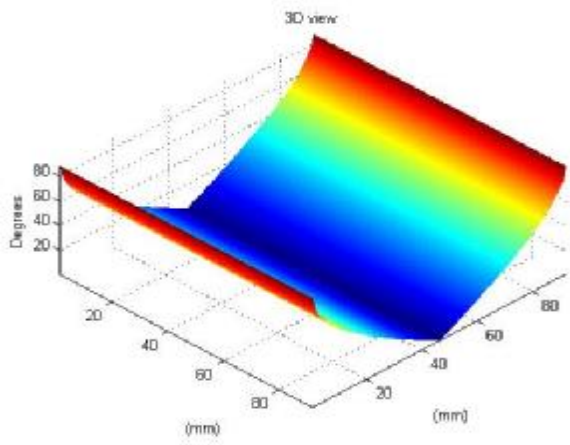

(a)

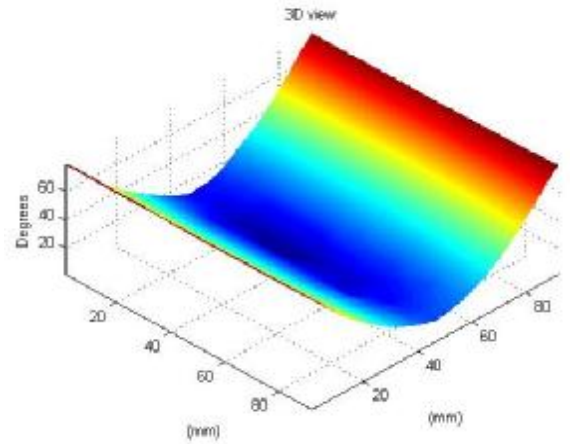

(b)

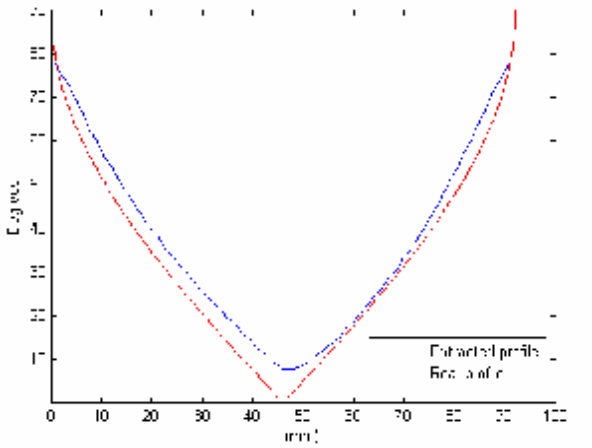

(c)

Fig.5: *A plexiglas hemicycle specimen: (a) real surface shape; (b) extracted surface shape; (c) mean profiles of (a) and (b).*

6. Conclusion

In this work we showed that the *blind frequency inversion method* in PPT is not affected by surface orientation of complex-shaped objects while amplitude images are indeed related to object surface shape. An approach of shape extraction was thus proposed based on amplitude images in PPT. This method called *shape from amplitude* was adapted from the method of "shape from heating" previously proposed.

Acknowledgments

The financial support provided by the Ministère des Relations Internationales du Québec (Scientific cooperation program Québec/Italy n° RST-RT 05.204), NSERC and Canada Research Chairs are gratefully acknowledged.

7. References

[1] Ibarra-Castanedo C., González D. A. and Maldague X., "Automatic Algorithm for Quantitative Pulsed Phase Thermography Calculations", CD of Proc. of WCNDT - World Conference on Nondestructive Testing, Montréal (QC, Canada), August 30 – September 4, 2004.

[2] Maldague X., Barker E., Nouah A., Boisvert E., Dufort B., Fortin L., "On Methods for Shape Correction and Reconstruction in Thermographic NDT", IInd International Workshop on Advances in Signal Processing for NDE of Materials, Kluwer Academic Pub., E - 262: 209-224, 1994.

[3] Pelletier J. F., Maldague X., "Shape from Heating: A Two-Dimensional Approach for Shape Extraction in Infrared Images," Optical Engineering, 36: 371-375, Feb. 1997.

[4] Maldague X., "Theory and Practice of Infrared Technology for Nondestructive Testing", John Wiley & Sons, Inc, pp. 1-4, pp.4, pp. 343-349, pp. 406-415, pp. 439-448, 2001.

[5] Fourier J., "Théorie du Mouvement de la Chaleur dans Les Corps Solides - 1ère partie", Mémoires de l'Académie des Sciences, 4:185-555, 1824; 5:153-246, 1826.

[6] Favro L. D., Han X., "Thermal Wave Material Characterization and Thermal Wave Imaging," in Sensing for Materials Characterization, Processing, and Manufacturing, G. Birnbaum, B. A. Auld eds., ASNT TONES 1: 399-415, 1998.

[7] Hutcheson, M. C., "Trimmed Resistant Weighted Scatterplot Smooth", Master's Thesis, Cornell University, Ithaca, N.Y., 1995.

[8] Shepard S., "Advances in Pulsed Thermography", A. E. Rozlosnik, R. B. Dinwiddie eds., Thermosense XIV, SPIE Proc., 4360: 511-515, 2001.